Tellus SERIES A DYNAMIC METEOROLOGY AND OCEANOGRAPHY
PUBLISHED BY THE INTERNATIONAL METEOROLOGICAL INSTITUTE IN STOCKHOLM

Tellus (2010), 62A, 481–496

TELLUS

Characteristics and impact of a gale-force storm field over the Norwegian Sea

By BURGHARD BRÜMMER[1], GERD MÜLLER[1]*, CHRISTIAN KLEPP[1], GUNNAR SPREEN[2], ROLAND ROMEISER[3] and JOCHEN HORSTMANN[4], [1]*Meteorological Institute, University of Hamburg, Germany*; [2]*Institute for Oceanography, University of Hamburg, Germany*; [3]*Rosenstiel School of Marine and Atmospheric Science, University of Miami, Miami, FL, USA*; [4]*Institute for Coastal Research, GKSS Research Center, Geesthacht, Germany*

(Manuscript received 27 July 2009; in final form 12 March 2010)

ABSTRACT

A unique data set was sampled by aircraft, ship, drift buoys and satellites in a strong storm event which occurred over the Norwegian Sea in March 2005 during the LOFZY field experiment. The atmospheric characteristics and the impact on the upper ocean are investigated. The storm field with winds up to 27 m s^{-1} was situated on the west-side of a low-pressure trough along the Norwegian coast and was marked by a sharp wind front. The entire system of trough, front and storm field was about 200 km wide, had a lifetime of 2 d in the area and advanced at 1–3 m s^{-1} SE-wards. Temperature contrast across the system was small, but wind contrast was remarkable and concentrated in a step-like front with 5–15 m s^{-1} difference over a distance of 3 km. The entire system was restricted to the lowest 2 km. It was accompanied by wide-spread rain and snow. Precipitation slightly surpassed evaporation (0.22 mm h^{-1}). Surface heat fluxes amounted up to 400 W m^{-2}. However, they cannot account for the observed sea surface temperature changes between −0.8 and +0.1 K within 6 h during the frontal passage. This is attributed to vertical mixing in the ocean caused by the frontal wind impact and superimposed to pre-existing mesoscale eddy circulations. The mixing acted on a temperature stratification in the uppermost 20–100 m which was opposite on both sides of the Norwegian Current.

1. Introduction

The Norwegian Sea is a region of the North Atlantic where cyclone frequency has a secondary maximum. The primary maximum is situated over the Irminger Sea, that is the region of the Icelandic low (e.g. Rogers, 1997; Brümmer et al., 2000; Affeld, 2003; Zhang et al., 2004; Tsukernik et al., 2007). In the long-term average of wintertime sea level pressure (SLP), a low pressure zone extends from the Icelandic low towards the Norwegian Sea. In some winters, the absolute SLP minimum within the North Atlantic low pressure zone can even be situated in this region (Rogers, 1997; Skeie, 2000; Cavalieri and Häkkinen, 2001; Jahnke-Bornemann and Brümmer, 2009). Furthermore, the Norwegian Sea is a region where latent heat flux and precipitation have relative maxima in winter. West of the Lofotes Islands the Norwegian Current which transports warm and salty Atlantic water masses northward towards the Arctic Ocean can reach velocities up to 1 m s^{-1} near the surface (Poulain et al., 1996). All these facts indicate that the Norwegian Sea is a region of intense atmosphere–ocean interaction in which cyclones play an important role (Sorteberg et al., 2005).

To study this interaction for individual cyclones was the main objective of the field experiment LOFZY (Lofotes Zyklonen) which took place in the area west of the Lofotes Islands in February and March 2005. In this paper, observations of a low-pressure trough which was aligned parallel to the Norwegian coast and of its impact on the underlying ocean are presented and analysed. This situation occurred on 12 and 13 March 2005 and is of particular interest for three reasons: (1) the low pressure trough was accompanied on its west side by an extended storm field (with winds up to 27 m s^{-1}) whose edge was marked by a sharp wind front, (2) the situation had a long (about 2 d) lifetime and residence time within the area and (3) the case is representative of a SLP distribution over the Norwegian Sea which occurs frequently in winter.

Comprehensive research exists on hurricanes and their interaction with the ocean (e.g. Schade and Emanuel, 1999; Zedler et al., 2002; Drennan et al., 2007; French et al., 2007). Also, there is much research on polar lows which have a high impact weather potential, but which are short-lived and mesoscale.

*Corresponding author.
e-mail: gerd.mueller@zmaw.de
DOI: 10.1111/j.1600-0870.2010.00448.x

Recently, Saetra et al. (2008) investigated the possible impact of polar lows on the ocean surface temperature. Interestingly, however, there is comparatively little research work on synoptic-scale cyclones and their associated storm fields in middle and high latitudes and their interaction with the underlying ocean (e.g. Pickart et al., 2003; Ren et al., 2004; Young et al., 2005). Several recent papers deal with the air–sea fluxes of momentum and heat under very high wind conditions in mid-latitude weather systems (e.g. Persson et al., 2005; Moore et al., 2008; Petersen and Renfrew, 2009). The involved impact of the weather systems on the upper ocean has not been studied. This requires simultaneous measurements both in the atmosphere and the ocean. This paper aims to contribute to this latter field by detailed observations which are based on a wide range of platforms including drift buoys, aircraft and ship measurements along with satellite remote-sensing data. The objectives of this paper are to analyse the atmospheric characteristics of the low-pressure trough and gale-force wind field and to quantify the related air–sea interaction processes and impact on the upper ocean.

The paper is organized as follows. In Section 2, the data sources are described. The synoptic-scale situation and temporal development are presented in Section 3. In Section 4, the atmospheric properties of the low-pressure trough, the gale-force wind field and the sharp wind front in the transition zone between both regions are analysed. Section 5 deals with the interaction processes between atmosphere and ocean and the impact on the ocean and conclusions are drawn in Section 6.

2. The observational data

The data for this study were taken on 12 and 13 March 2005 during the LOFZY field experiment (the intensive phase lasted from 27 February until 22 March 2005) by drift buoys, the German research aircraft Dassault Falcon-20, the Irish research vessel (R/V) Celtic Explorer and various satellite instruments.

At the beginning of LOFZY, 23 drift buoys of the type XAN-1 manufactured by the Canadian company Metocean were deployed to the west of the Lofotes Islands within a rectangle of about 400 km × 650 km with its centre at 70°N, 10°E. Eighteen buoys were deployed by a transport aircraft and five buoys by R/V Celtic Explorer. Two buoys did not function after dropping from the aircraft. XAN-1 buoys measured position, SLP, surface air temperature (SAT) at 0.6 m height and sea surface temperature (SST) at 0.4 m depth at about hourly intervals and transmitted the data via the ARGOS satellite system. Most buoys operated until September 2005. The buoy positions on 12 and 13 March are shown in Fig. 1.

The research aircraft Falcon of the German Aerospace Centre in Oberpfaffenhofen, Germany, participated from 2 to 22 March 2005 in the experiment and operated from the airfield of Andenes (69.3°N, 16.1°E) on Andöya Island. The Falcon was equipped with sensors for high-frequency turbulence (sampling rate 100 Hz) measurements of three-dimensional wind vector, temperature and humidity from which turbulent fluxes of sensible heat, latent heat and momentum were calculated. Furthermore, short- and long-wave up- and downward looking radiometers for net radiation flux as well as an infrared sensor for SST and a liquid water content probe were installed. In total eight flight missions in eight different cyclone conditions were conducted during the experiment. The mission on 12 March is analysed in this paper and consisted of low-level runs and vertical profiles to document the three-dimensional atmospheric structure. Low-level runs were flown at 30 m height as long as weather and visibility conditions allowed for that. The flight pattern is shown in Fig. 1.

R/V Celtic Explorer operated in the LOFZY area (defined by the initial area of the buoy array) from 27 February to 19 March 2005. During this time the ship surrounded the area two times. Basic meteorological quantities were measured continuously aboard the ship and recorded as one-minute averages and radiosondes were launched every 3 h. In addition, oceanographic parameters were profiled continuously by an Acoustic Doppler Current Profiler (ADCP) and at specified locations by a conductivity, temperature, depth (CTD) instrumentation. The positions of R/V Celtic Explorer on 12 and 13 March are shown in Fig. 1. The complete ship's track is shown in Fig. 13.

In addition to the in situ measurements, several standard and specifically generated data products of remote sensing satellites are used in this study to obtain comprehensive meteorological and upper ocean information in the experimental area. The satellite data comprise visible and infrared images from the NOAA-AVHRR sensor and radar- and microwave-based wind fields either as standard products from SeaWinds on QuikSCAT or as products from ENVISAT-ASAR and SSM/I by applying specific wind retrieval algorithms.

The SeaWinds instrument on the QuikSCAT satellite of NASA is a wind scatterometer. Wind speed and direction are retrieved from the microwave reflectivity of the ocean surface at 13.4 GHz. The swath width of SeaWinds is 1800 km and the spatial resolution of the Level 2B swath wind data used here is 25 km. QuikSCAT wind data with a good coverage of the LOFZY experimental area on 12 March 2005, the main day of this study, are available at 02.52, 04.30, 18.10 and 19.50 UTC.

The Advanced Synthetic Aperture Radar (ASAR) on the satellite ENVISAT of ESA is an imaging radar (5.3 GHz) with various possible modes of operation. Here ASAR wide swath mode (ScanSAR) data with a nominal resolution of 150 m are used. ASAR images for specific purposes and areas need to be ordered in advance. For the LOFZY experimental area, a total of 17 images were acquired for the period 28 February to 22 March 2005. A wide swath ASAR image is available on 12 March 2005 at 20.41 UTC which covers an area of 375 km × 375 km in the study region.

Using radiances of the Special Sensor Microwave/Imager (SSM/I) radiometers, a total of 15 parameters is derived in the HOAPS (Hamburg Ocean Atmosphere Parameters and Fluxes

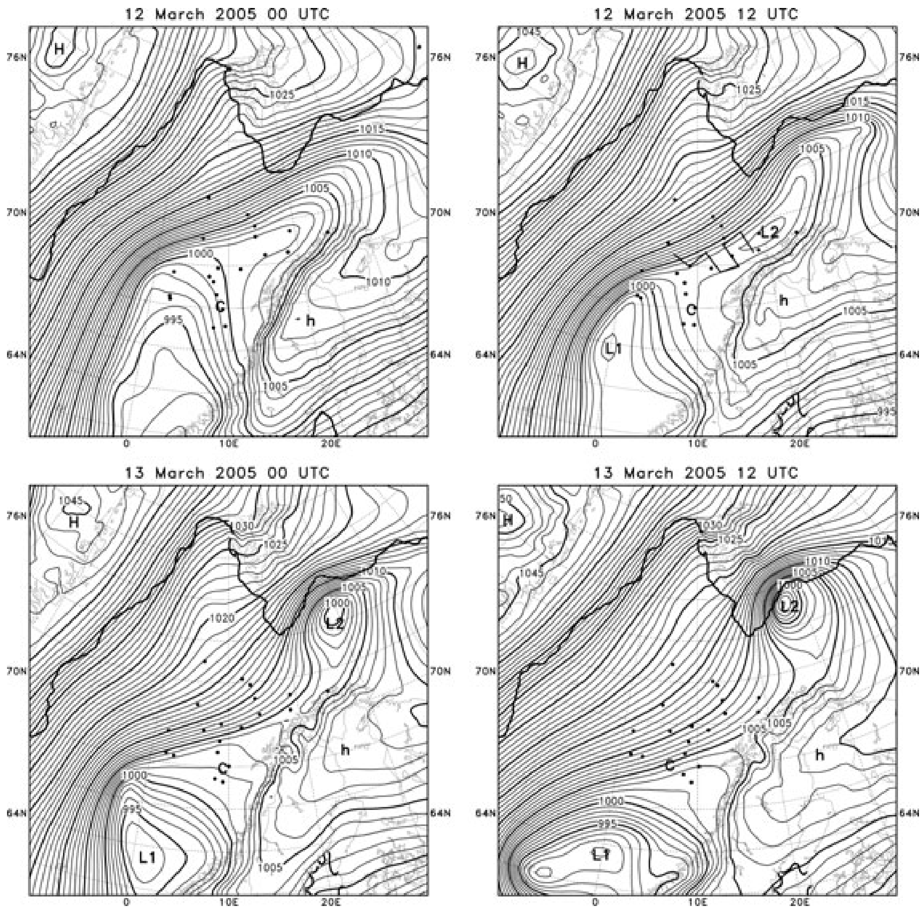

Fig. 1. Twelve-hourly ECMWF sea level pressure fields on 12 and 13 March 2005 with cyclones L1 and L2 developing within the trough to the W of the Norwegian coast and with positions of XAN-1 buoys (dots), R/V Celtic Explorer (C) and research aircraft Falcon flight pattern (straight lines upper right panel).

from Satellite Data) climatological data set which is described in Andersson (2009) and is freely available. In this paper, the HOAPS parameters, wind speed, precipitation and evaporation, are used.

3. Large-scale weather situation

The synoptic situation on 12–13 March 2005 is demonstrated in Fig. 1 by a series of 12-hourly ECMWF SLP analyses which have a horizontal resolution of 0.25°. Lammert et al. (2008) used LOFZY buoy data to validate the operational analyses of the European Centre of Medium-Range Weather Forecast (ECMWF). They obtained a value of 0.99 for the correlation between the buoy SLP measurements and the ECMWF SLP analyses. This demonstrates a high degree of reality of the ECMWF SLP analyses in Fig. 1, at least on the synoptic scale.

On 12 March 2005 at 00 UTC a large low pressure system was situated with its core (about 981 hPa) over the southern Baltic Sea (not shown in Fig. 1). From there, a long trough extended over the North Sea and along the Norwegian coast. Along the trough line SLP gradients were generally weak, but to the west of the trough, SLP increased steeply towards a high over Greenland (1045 hPa). As will be shown below, the increase of SLP gradient to the west of the trough was marked by a sharp boundary, called wind front here. Until 12 March at 12 UTC this situation remained nearly unchanged. Two small low pressure cores (L1, L2) developed in the trough line: L1 near 68°N, 0°E and L2 north of the Lofotes Islands. The wind front in the area west of the Lofotes Islands advanced only slowly SE-wards. Until 13 March at 00 UTC, the two SLP cores deepened to well-developed cyclone centres (L1, L2) and continued to deepen. The northern cyclone centre, L2, moved NE-ward into the Barents Sea and the southern cyclone centre, L1, S-ward. The trough line connecting both cyclone centres was still situated west of the Norwegian coast and became very narrow in the region to the north of the Lofotes Islands. The wind front propagated further towards SE. Until 13 March at 12 UTC this large-scale flow situation did not change significantly. The low pressure line

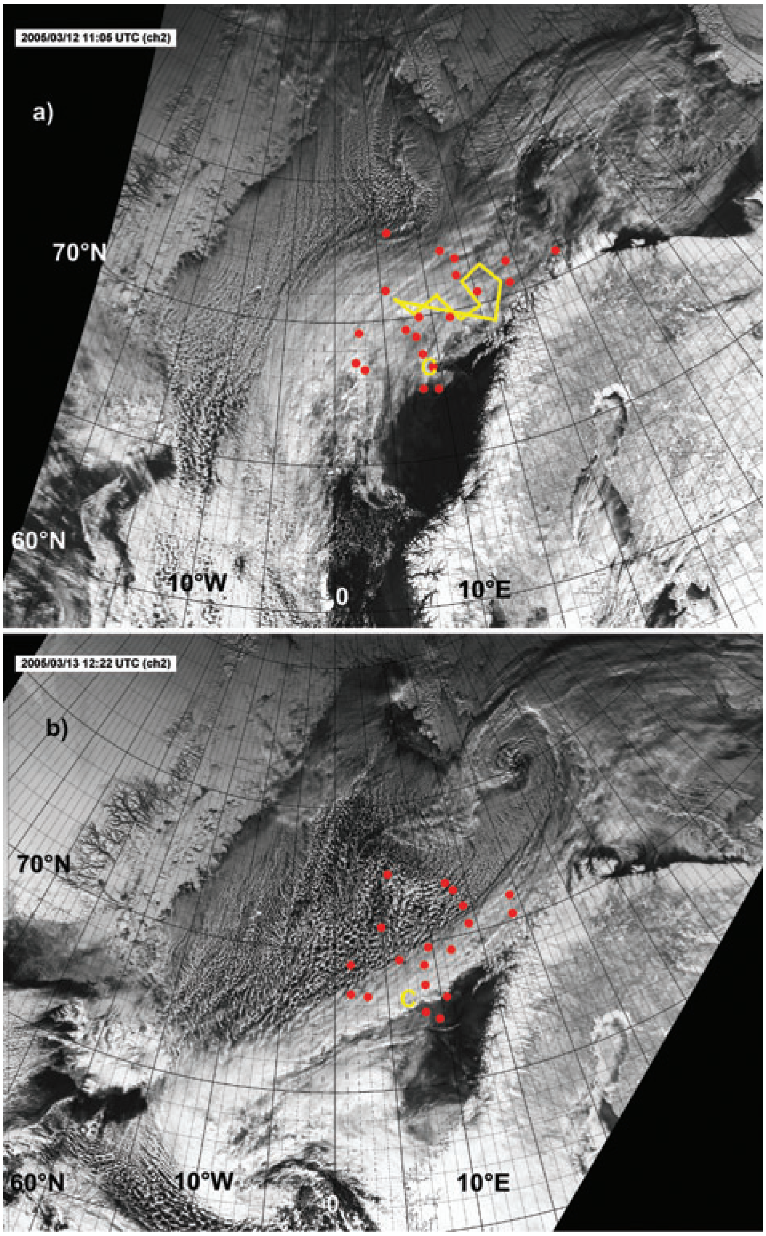

Fig. 2. NOAA AVHRR satellite images (visible channel 2) on 12 March 2005 at 11.05 UTC (a) and on 13 March 2005 at 12.22 UTC (b) with positions of XAN-1 buoys (dots), R/V Celtic Explorer (C) and research aircraft Falcon flight pattern (straightlines).

with the wind front on its west side reached the Norwegian coast at 70°N. The SLP gradient to the west of the wind-front slightly weakened.

The cloud fields associated with the low pressure trough are illustrated in Fig. 2 by two NOAA AVHRR satellite images. The AVHRR image on 12 March 2005 at 11.05 UTC shows a broad not yet well-organized field of high level clouds over the western and northern part of the Norwegian Sea. The just developing L1 and L2 SLP minima were situated below this extended cloud field. In the western part the high level clouds appear to shield the lower cellular convective clouds of the cold-air outbreak from the north. To the west of Middle-Norway and on the eastside of the trough, a nearly cloudfree area was present. Together with the southeasterly winds in this area (Fig. 1), this hints at a Föhn effect in the lee of the Norwegian mountains. The AVHRR image was taken during the middle of the Falcon flight mission and is, thus, representative of the time period of the aircraft measurements. The satellite image on 13 March 2005 at 12.22 UTC (Fig. 2b) was taken 25 h later, at a time when both lows L1 and L2 were already well-developed and separated further in different directions. The image shows a well-organized cloud band along the low pressure trough connecting both cyclone centres. The wind front was located at the SE edge of the cloud band and has just passed the position of R/V Celtic Explorer.

4. Structure and characteristics of trough and wind front

Based on the latest analyses and forecasts from several operational weather services, the Falcon flight mission on 12 March 2005 was planned. It took place between 09.40 (take-off) and 12.40 UTC (landing). The flight pattern consisted of 9 low-level horizontal runs (abbreviated by H1–H9) and 11 vertical profiles (abbreviated by P1–P11). Their locations are indicated in Fig. 3. Runs H3, H5, H7 and H9 intersected the trough line at four different locations, while runs H1, H2 and H6 were located south of the trough and runs H4 and H8 north of the trough. Profiles were taken on both sides of the trough: profiles P1, P2, P3, P6, P7 and P11 south of it and profiles P4, P5, P8, P9 and P10 north of it. The originally planned flight pattern consisted of four regular rectangular trough intersections. However, during the flight along H8 it turned out that the trough was not a straight line as indicated by the available forecasts, but was curved within the flight area, so that the flight plan was changed in the way as given in Fig. 3. A complete fourth low-level rectangular intersection of the trough was not possible because the aircraft endurance limit was reached.

Using data from all aircraft low-level runs, all buoys and all available synoptic stations, the resulting SLP, SST and wind distributions in the experimental area for 12 UTC on 12 March 2005 are displayed in Fig. 3. The wind front is marked as the position where the aircraft wind exceeded the level of 10 m s^{-1} and where the strong SLP gradients began, elsewhere. Wind front and trough line did not coincide in position; the wind front was clearly located to the north of the trough. At this time, 12 UTC, the whole system (front and trough) was situated over the warmest part of the Norwegian Current.

The trough line was not associated with a large temperature contrast, but only with a distinct contrast in wind direction and speed. This is demonstrated in Fig. 4 by Falcon profiles on both sides of the trough. Profile P3 taken on the southeast side of the trough, but over the cooler coastal water had almost the same temperature in the lowest 500 m as profile P10 taken north of the trough on the other side of the Norwegian Current, but over similar SST. Due to unstable air–sea temperature stratification a well-mixed boundary layer was present everywhere in the area, so that the air temperature contrasts across the trough were small not only near the surface but also at higher levels: they amounted to 0–2 K below 500 m (average cloud base outside of showers), increased to 1–4 K between 500 and 1800 m and were almost negligible again (0–2 K) further above. On the other hand the wind contrast was clearly outstanding with southerly wind of 5–10 m s^{-1} south of the trough and northeasterly wind of 15–25 m s^{-1} north of the trough. This was true for the lowest 500 m. Above this layer, the wind decreased to less than 5 m s^{-1} and turned to northeasterly direction on the south side of the trough. On the north side of the trough the strong northeasterly wind extended up to 1500 m height and decreased above that. Winds were small everywhere above 2 km height. Thus, the gale-force wind field and the corresponding wind front were a phenomenon of the lowest 1.5–2 km only.

The detailed transition of the wind across the trough and the wind front was measured along the four aircraft runs H3, H5,

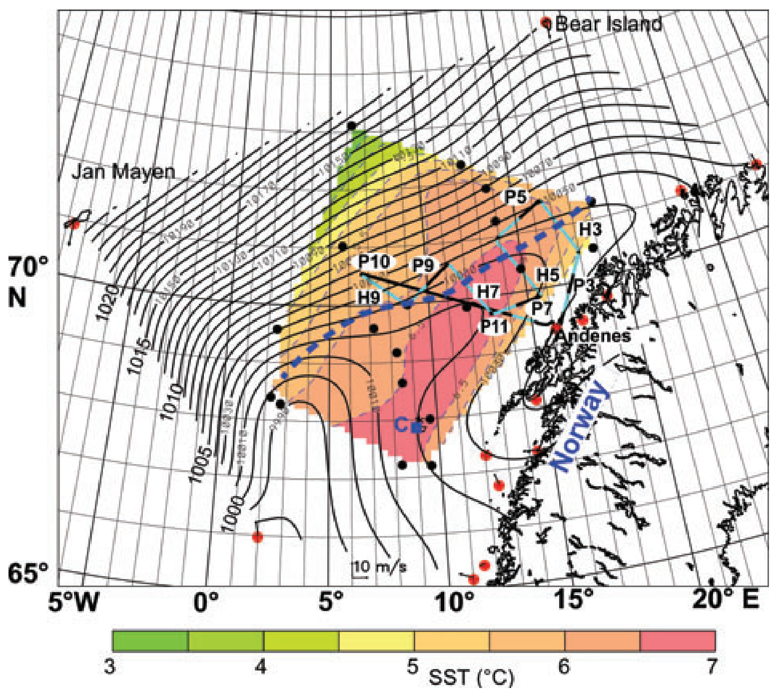

Fig. 3. Sea-level pressure distribution on 12 March 2005 at 12 UTC as measured by XAN-1 buoys (black dots), synoptic weather stations (red dots), R/V Celtic Explorer (C) and research aircraft Falcon (low-level runs are shown in blue) as well as sea-surface temperature distribution as measured by XAN-1 buoys. Falcon horizontal runs (H3, H5, H7 and H9) and vertical profiles (P3, P5, P7, P9, P10 and P11) which are referred to below are marked. The thick dashed line gives the position of the wind front.

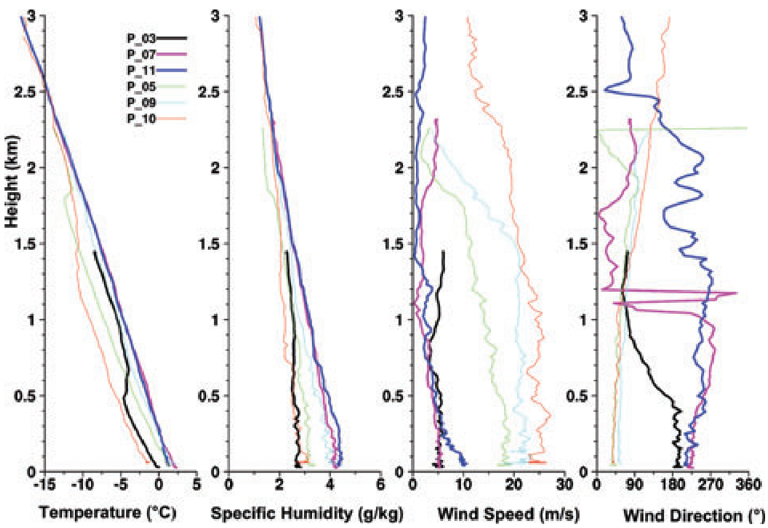

Fig. 4. Vertical profiles of temperature, specific humidity, wind speed and wind direction measured by research aircraft Falcon measured on the southside (P3, P7 and P11) and northside (P5, P9 and P10) of the trough. Profile locations are shown in Fig 3.

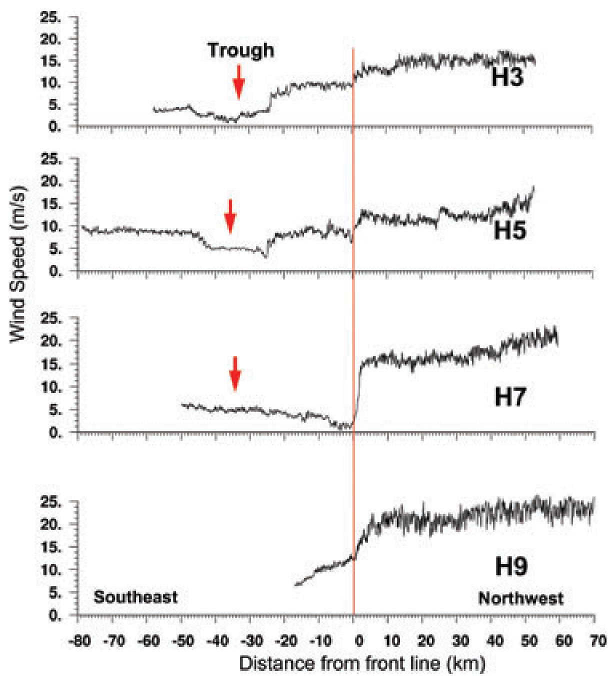

Fig. 5. Wind speed as measured by research aircraft Falcon during the wind front intersections along the low-level runs H3, H5, H7 and H9 (locations are shown in Fig. 3). The wind front is located at zero distance. Arrows mark position of lowest sea level pressure within the trough.

H7 and H9 and is displayed in Fig. 5. The runs refer to 30–60 m height and are arranged with respect to the main wind front which is defined as the position where the 10 m/s level is exceeded. The wind transition was not uniform, but occurred in steps of different wind speed (FF) contrast ΔFF and horizontal width Δx. There were two wind steps in H3 and H5 and one wind step in H7 and H9. The different form of wind transition was caused by a small subsynoptic SLP minimum embedded within the trough line as was measured by the aircraft, but which does not appear in the ECMWF analysis in Fig. 1. In Table 1 the characteristics of the wind front are summarized. This includes the width Δx (defined by the beginning and end of the strong wind gradient), the wind speeds FF and directions DD ahead and behind the front and the front orientation α, from which the front-parallel and front-normal wind components (U_p, U_n) are determined and the cross-frontal wind shear, $\Delta U_p/\Delta x$ and the cross-frontal wind convergence, $\Delta U_n/\Delta x$, are calculated. The cyclonic wind shear amounts to 0.5–4.7 × 10^{-3} s^{-1} and the wind convergence amounts to –1.1 to –2.5 × 10^{-3} s^{-1}.

During the three runs H3, H5 and H7 which intersected both, the wind front and the trough, the wind front was located about 30–40 km to the north of the trough line. The strongest winds with 27 m s^{-1} were measured at the uttermost end of H9. There, also the largest air–sea instability with –6 to –7 K occurred and the differences between maximum and minimum wind speeds were more than 10 m s^{-1}. It must be underlined that in-situ data sampled under these extreme weather conditions at low levels of 30–60 m are rather rare (e.g. Drennan et al., 2007; French et al., 2007; Petersen and Renfrew, 2009) and that this success was only possible due to the extraordinary efforts of the Falcon pilots.

In Fig. 6a–c three HOAPS DMSP, SSM/I satellite scenes taken at 09.49, 18.08 and 19.49 UTC on 12 March 2005 reveal the wind speed distribution beyond the area of the aircraft mission which started almost at the time of the first HOAPS scene. The wind fields demonstrate the existence of a sharp, coherent wind front. They support the aircraft and buoy findings of an S-shaped front orientation (α) (see Figs 3 and 12, respectively) and that the cross-frontal wind transition was not homogeneous along the front. On the high-wind side of the front the wind speed increased from NE to SW and was largest in the area to the NW of cyclone L1. On the low-wind side of the front the wind distribution

Table 1. Characteristics of the wind front as measured during the four aircraft intersections H3, H5, H7 and H9: width Δx, front orientation α, wind speed FF, wind direction DD, front-parallel wind component U_p, front-normal wind component U_n, cross-frontal wind shear $\Delta U_p/\Delta x$ and cross-frontal wind divergence $\Delta U_n/\Delta x$.

Parameter	H3	H5	H7	H9
Δx (km)	3.0	3.0	2.7	3.0
α (°)	65 ± 5	65 ±5	70 ± 5	70 ± 5
FF (m s^{-1}); DD (°) ahead front	9.0 ± 1.0; 65 ± 10	8.5 ± 2.0; 100 ± 5	1.0 ± 1.0; 170 ± 20	11.5 ± 1.0; 70 ± 3
FF (m s^{-1}); DD (°) behind front	13.0 ± 1.0; 30 ± 5	13.0 ± 1.5; 70 ± 10	14.0 ± 1.5; 60 ± 3	20.5 ± 2.5; 60 ± 3
U_p; U_n (m s^{-1}) ahead front	9.0; 0.0	7.0; 4.9	−0.2; 1.0	11.5; 0.0
U_p; U_n (m s^{-1}) behind front	10.6; −7.5	12.9; 1.1	23.8; −2.4	20.2; −3.6
$\Delta U_p/\Delta x$ (10^{-3} s^{-1})	0.5	2.0	4.7	2.9
$\Delta U_n/\Delta x$ (10^{-3} s^{-1})	−2.5	−1.3	−1.1	−1.2

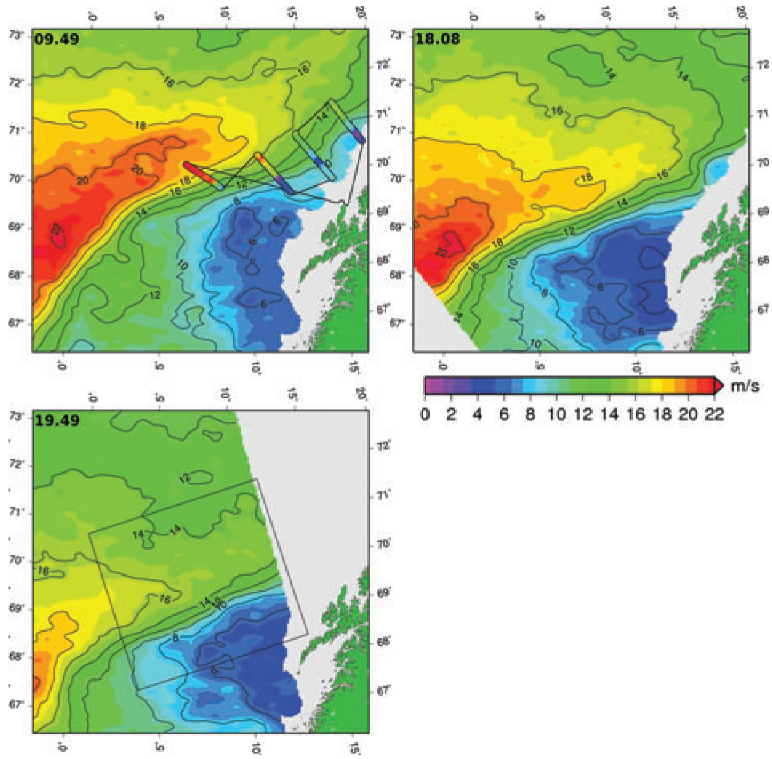

Fig. 6. Wind speed distribution as retrieved from HOAPS SSM/I-F15 at 09.49, 18.08 and 19.49 UTC on 12 March 2005. For 09.49 UTC the Falcon flight pattern and measured wind speeds for flight legs H3, H5, H7 and H9 are shown. For 19.49 UTC the position of the ENVISAT ASAR image in Fig. 7 is marked for reference.

exhibited patches of higher and lower wind speed presumably associated with small local SLP minima within the trough line as found by the aircraft. Fig. 6 shows that the front had a long lifetime and a small propagation speed of 0.5–1.5 m s^{-1}. Thus, the impact of the front and the following storm field on the ocean lasted for a rather long time. The absolute wind values retrieved from HOAPS and measured by aircraft do not agree everywhere, especially in the high wind speed zones. This is mainly due to the different heights the wind speeds were measured. The HOAPS data represent winds in 10 m height, while the Falcon aircraft flew in between 30 and 60 m height. For a direct comparison the two wind measurements would have to be adapted to the same reference height (Fairall et al., 2003). The time difference of up to 2 h for the western part between the Falcon H9 run and the SSM/I-F15 overpass and the HOAPS retrieval algorithm for high wind speeds could likely cause additional discrepancies, which would have to be corrected for. Here, we are, however, only interested in relative differences in and around the wind front and it is not the scope of this paper to make a quantitative wind speed comparison between the two data sets.

The HOAPS wind scenes cover a large region of the experimental area, but have a resolution of only 50 km. To get more information on the small-scale features of the wind front we use the only available ASAR image that covers the experimental area on this day at 20.41 UTC. It is shown in Fig. 7 and its position is also marked in Fig. 6c. Fig. 7a shows the radar backscatter

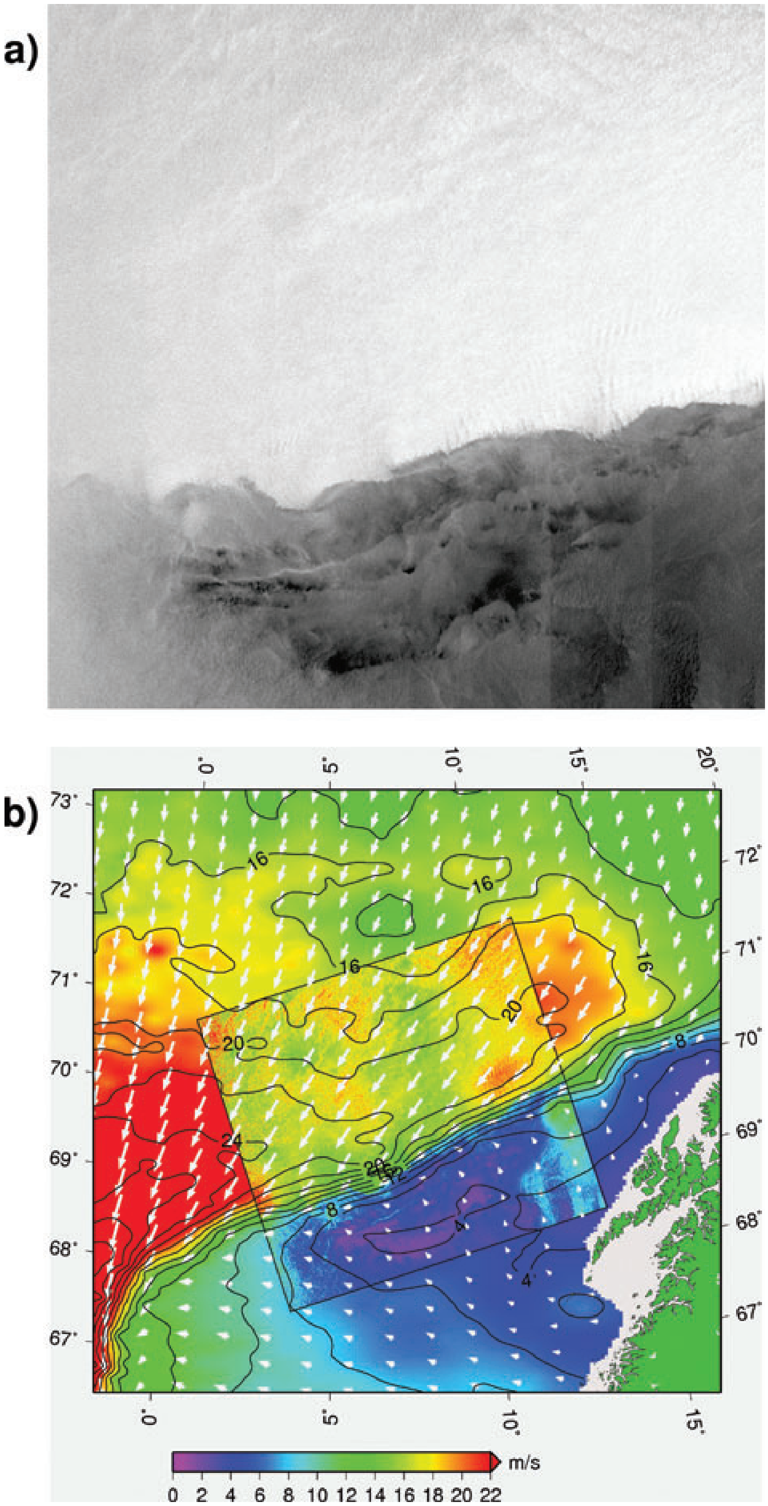

Fig. 7. (a) Radar backscatter intensity as measured by ENVISAT ASAR at 20.41 UTC on 12 March 2005. The location of the image is marked in Fig. 7b. (b) Distribution of wind speed and wind direction as retrieved from QuikSCAT (19.49 UTC, large frame) and from ENVISAT ASAR (20.41 UTC, small frame). Despite of differences due to different retrieval algorithms, both images show the sharp wind shear along the more than 1000-km-long wind front.

intensity. Fig. 7b shows the ASAR wind speed retrieved using an algorithm of Horstmann and Koch (2005) together with a QuikSCAT wind scene for 19.50 UTC which is underlaid. Additionally QuikSCAT wind vectors are overlaid in Fig. 7b. The general potential of satellite SAR as a tool to detect meteorological fronts and their finescale structures was demonstrated by Young et al. (2005). The ASAR image supports the aircraft observation of the sharpness of the wind front with a width of about

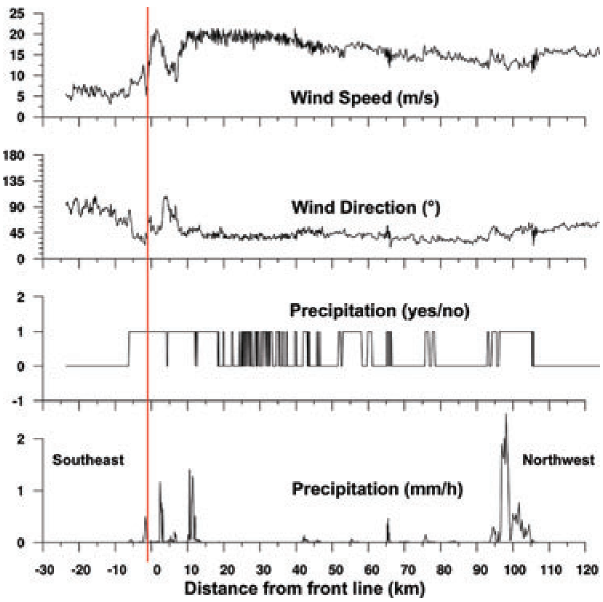

Fig. 8. Wind speed, wind direction and precipitation from a precipitation indicator (yes/no) and an optical precipitation disdrometer measured aboard R/V Celtic Explorer between 13 March at 06 UTC and 14 March 06 UTC. The time series was translated via ship's speed and frontal speed and orientation to a distance relative to the front.

2 km. Furthermore, it shows meander-like deformations of the front with a wavelength around 50 km and superimposed front-normal wave lines with about 5 km wavelength in the east part of the image. The reasons for both wave features cannot be analysed from the available observational data, but are likely related to the strong frontal wind shear as given in Table 1. Fig. 7b shows that the two satellite retrieved wind fields (ASAR, QuikSCAT) do not agree in every detail (mean difference about 1.7 m s^{-1}), especially in the high wind speed region. This is in line with findings of Renfrew et al. (2009) and Moore et al. (2008), who observe a tendency of the used QuikSCAT algorithm to overestimate wind speeds above $\sim$18 m s^{-1} in comparison to buoy and aircraft data. The ASAR-derived and HOAPS wind speeds are much closer together (mean difference: -0.4 m s^{-1} using the 19.49 UTC HOAPS wind field in Fig. 6). A more detailed study to analyse the observed differences between QuikSCAT, HOAPS and the Falcon aircraft measurements is underway.

Twelve hours after the ASAR image was taken the wind front reached R/V Celtic Explorer on 13 March at 09.10 UTC. From the elapsed time a propagation speed of $c = 2$–4 m/s and an orientation of $\alpha = 60$–$70°$ is estimated. Wind and precipitation measured aboard the R/V are displayed in Fig. 8. Since the R/V Celtic Explorer was not stationary, but steamed towards WNW with some intermediate stops for radiosonde and CTD measurements, the time t has been translated to a distance x in front-normal direction via

$$\Delta x = (c + c_{n,\mathrm{RV}})\Delta t,$$

with $c = 3$ m s^{-1} and $c_{n,\mathrm{RV}} = c_{\mathrm{RV}} \cos(\alpha_{\mathrm{RV}} - 335°)$, where c_{RV} and α_{RV} are ship's speed and course, respectively. Fig. 8 shows that the wind front still existed with almost the same wind contrast from 5 to 20 m s^{-1} as measured 22 h before by the research aircraft Falcon. At the position of R/V Celtic Explorer the front had a double structure with a gale-force wind band preceding the main storm field. Radiosondes launched at 08.16 UTC ahead of the front, at 09.22 UTC in the preceding wind band and at 11.00 and 11.51 UTC in the main wind field (not shown here) support the aircraft findings that the temperature contrast across the front was small and that the wind contrast existed only in the lowest 1.5–2.0 km deep layer.

The system of trough, wind front and storm field existed for about 2 d (12 and 13 March 2005) in the LOFZY experimental area. The six-hourly ECMWF analyses of SLP and the twice-daily HOAPS wind climatology show that the system was generated over the Greenland Sea almost 2 d before, so that the total lifetime was nearly 4 d.

5. Impact of the wind front and storm field on the ocean

Wind front and storm field impact the ocean via surface stress τ, sensible heat flux H, latent heat flux (evaporation) E, precipitation P and net radiation R_n and, thus, change the currents, temperature and salinity of the ocean. In this section, the measurements of the impacting process quantities τ, H, E, P and R_n are presented and the impact on SST and ocean current is analysed.

5.1. Impacting processes

The turbulent fluxes of τ, H and E and the net radiation flux R_n as measured by the research aircraft Falcon are presented in Figs 9a–d. The turbulent fluxes were calculated from the 100 Hz data of three-dimensional wind u, v and w, temperature T and specific humidity q via the eddy covariance method as $\tau = -\rho\overline{w'u'}$, $H = \rho c_p \overline{w'T'}$ and $E = \rho L \overline{w'q'}$, where ρ is air density, c_p specific heat, L latent heat and the overbar and prime denote horizontal average and deviation from the average, respectively. The horizontal average is taken here over a 4 km length interval. Fluxes were also calculated over 2 and 8 km intervals resulting in only minor differences between each other. The net radiation flux was calculated from the individually measured up- and downwelling long- and shortwave radiation fluxes as $R_n = S\downarrow - S\uparrow + L\downarrow - L\uparrow$.

Surface stress follows more or less wind velocity and increased step-like at the wind front and then further towards NW with the increasing wind. The maximum values around $\tau = 1.15$ N m^{-2} were measured at the uttermost end of run H9. If an Ekman current in the ocean were forced by the surface stress, the current would be divergent particularly at the wind front, but also in the trough line and further to the NW of the front,

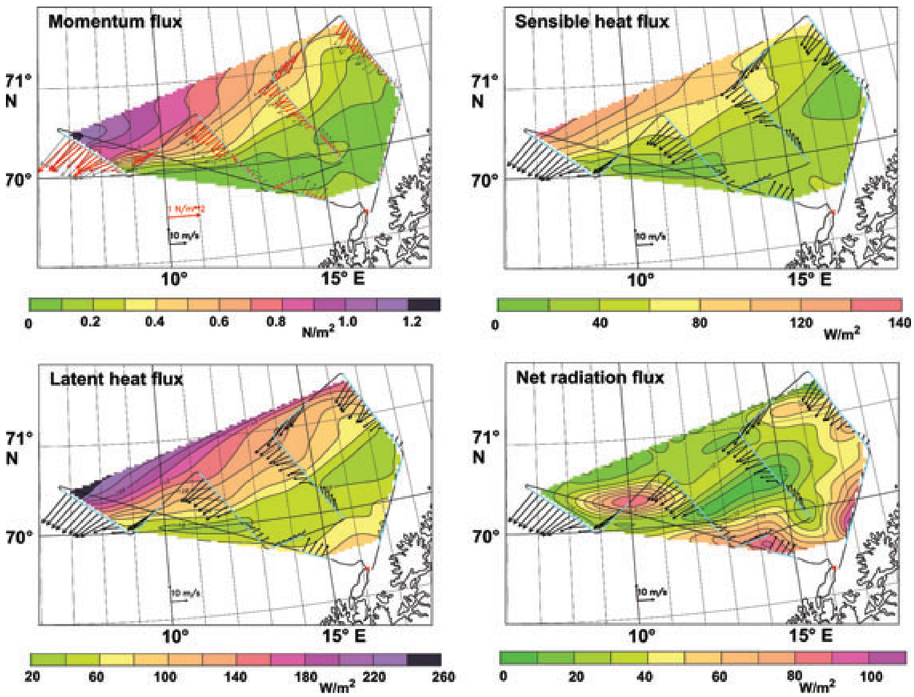

Fig. 9. Momentum flux, sensible heat flux, latent heat flux and net radiation flux as measured by research aircraft Falcon along all low-level runs. The wind field is also given for reference of the trough and wind front positions.

thus, resulting in a general upwelling. However, looking at details of the surface stress distribution along the flight pattern one can detect regions with either a confluent or a diffluent stress vector which would result in local deviations from the general upwelling on scales below 10–20 km.

The sensible heat flux was small ($H = 20$ W m^{-2}) along the trough line and increased towards N and S (Fig. 9b). The largest values of $H = 150$–160 W m^{-2} were measured at the end of run H9. The same horizontal distribution holds for the latent heat flux E (Fig. 9c), but both minimum and maximum values of E were higher than those of H and amounted to 30 and 260 W m^{-2}, respectively. Thus the largest energy loss of the ocean by the turbulent heat fluxes was 410 W m^{-2} in the aircraft area. The net radiation flux R_n (Fig. 9d) was very patchy because it depends strongly on the cloud conditions. Averaged over the entire aircraft area, R_n amounted to 41 W m^{-2}. Regarding only the long-wave fluxes as during the night, the average R_n would be -19 W m^{-2}. Assuming that during this time of the year day- and night-time conditions represent 40 and 60% of the day, the overall R_n is on the order of 5 W m^{-2} and, thus, is small compared to H and E.

Precipitation occurred widely spread in the trough, the wind front and the storm field area. This is demonstrated in Fig. 10 by the liquid water content (LWC) measurements during the four Falcon wind front trans-sections H3, H5, H7 and H9. LWC was measured with a Johnson–Williams instrument which is an open wire sensor. Since the transsections were below cloud base the measured LWC can be interpreted as precipitation.

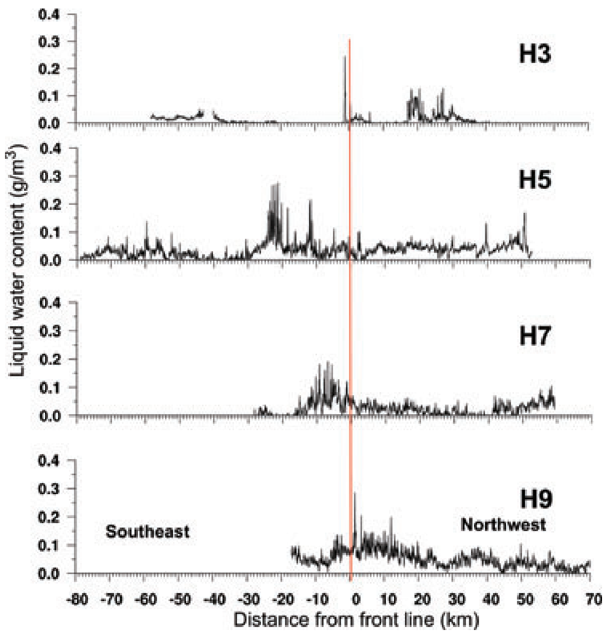

Fig. 10. Liquid water content as measured by research aircraft Falcon during the four wind front intersections along the low-level runs H3, H5, H7 and H9.

Quantitative LWC values have to be taken with some caution and may by uncertain by ±20%. Nevertheless, LWC measurements show that, except for some interruptions, precipitation occurred widely spread and was locally shower-wise intensified as was

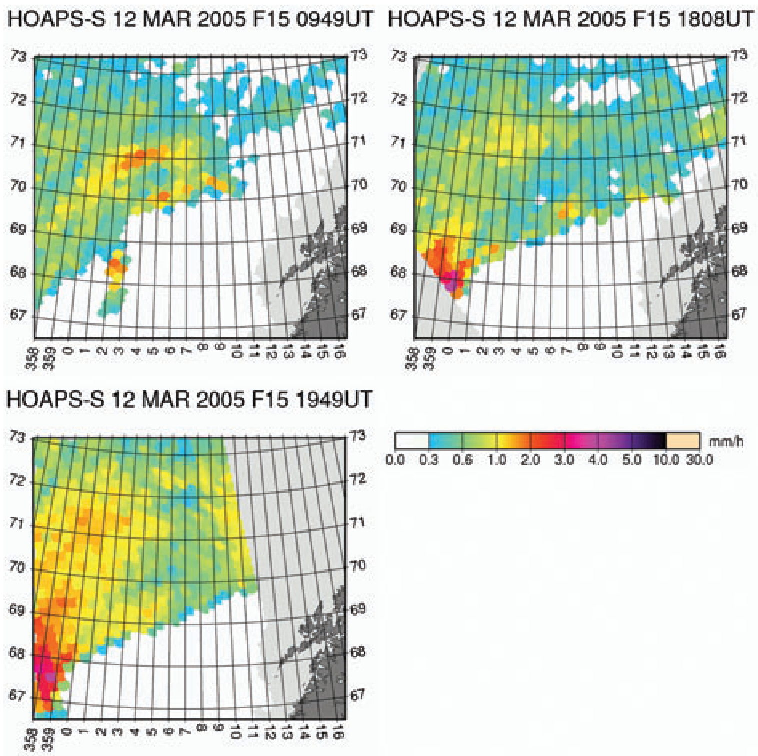

Fig. 11. HOAPS retrieved precipitation in mm h^{-1} from SSM/I-F15 satellite overpasses at 09.49 (including the flight pattern as a red curve), 18.08 and 19.49 UTC on 12 March 2005 in original resolution. Light grey colour represents no measurements and white colour values below the HOAPS retrieval threshold of 0.3 mm h^{-1}.

also measured at R/V Celtic Explorer in Fig. 8. Precipitation occurred as rain and as snow at air temperatures around 0 °C. If we assume that one half of the precipitation falls as rain with a descent rate of 6 m s^{-1} and the other half as snow with a descent rate of 1 m s^{-1} and if we take the mean LWC averaged over all four runs H3, H5, H7 and H9 (LWC = 0.032 g m^{-3}) we obtain an average precipitation rate of $P = 0.35$ mm h^{-1}.

Measurements by a precipitation detector and an ODM 470 optical disdrometer aboard R/V Celtic Explorer are displayed in Fig. 8. They show that the double-front passage was accompanied by almost continuous but light precipitation which intensified during the individual passages of the two wind fronts with values up to 1.2 and 1.4 mm h^{-1} falling in snow showers, according to the observer's log. In the main storm field mostly shower-like precipitation of less intensity was present except for a strong shower around mid-night from 13 to 14 March 2005.

The HOAPS precipitation with embedded shower intensifications is shown in Figs 11a–c for the same SSM/I-F15 satellite overpasses as shown in Fig. 6. The HOAPS retrieved precipitation is between 0.3 and 2.5 mm h^{-1} with an average value of about 0.38 mm h^{-1} and therefore compares well to the R/V Celtic Explorer and Falcon estimates. The satellite data demonstrate the long lifetime not only of the storm field but also of the precipitation field. The precipitation measurements aboard R/V Celtic Explorer were collocated against the HOAPS precipitation retrieval (point versus area measurement). On 13 March four satellite overpasses could be collocated to the ship's disdrometer data during the front passage with (ship/HOAPS) values in mm h^{-1} of (0.29/0.35), (0.29/0.33), (0.51/0.40) and (0.63/0.51). Overall results for LOFZY 2005 show, that the correlation between the disdrometer and the satellite data reaches 0.96 for 171 collocated events (Klepp et al., 2010).

The aircraft-based areal average precipitation estimate of $P =$ 0.35 mm h^{-1} (0.38 mm h^{-1} in HOAPS) is compared with the evaporation E/L, where E is the latent heat flux and L is the latent heat of evaporation. In Fig. 9c, the measured E varies between 30 and 260 W m^{-2}. If we average linearly between both values to estimate the areal mean we come up with $E = 145$ W m^{-2} which corresponds to an evaporation of $E/L = 0.22$ mm h^{-1}. The HOAPS evaporation is about 0.20 mm h^{-1}. Thus, precipitation surpasses evaporation, $P–E/L = 0.13$ mm h^{-1} (0.18 mm h^{-1} in HOAPS), and the entire weather system, i.e. trough, front and storm field together, is a weak positive freshwater event for the ocean. Assuming that the system is 200 km wide and advances with $c = 3$ m s^{-1} the net freshwater supply at each location is about 2 mm (3 mm in HOAPS).

5.2. *Impact on SST and drift*

To analyse the impact of the wind front on the ocean, we look at the buoy measurements in more detail. Fig. 12 shows the buoy positions on 12 March at 12 UTC and the average SST for this day. The position of the front was well documented by the aircraft measurements (Fig. 5). Since the front advanced slowly,

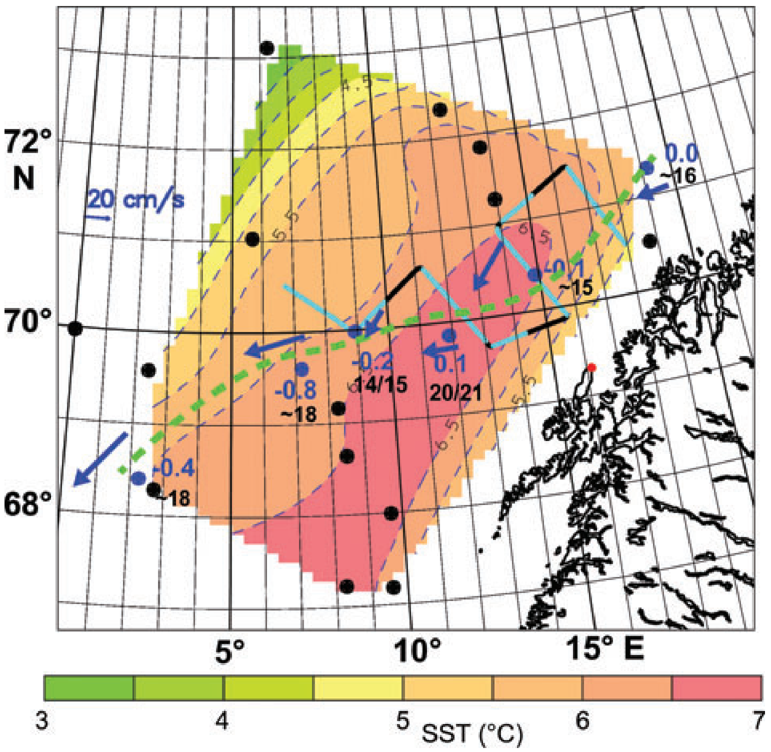

Fig. 12. Average sea-surface temperature distribution on 12 March 2005 measured by XAN-1 buoys (black and blue dots). Overlaid are the changes of sea-surface temperature (in K; blue numbers) and of near-surface drift vector (blue arrows) observed within 6 h at six buoys (blue dots) over which the wind front passed in the afternoon of 12 March. The drift difference vector is displaced from the respective buoy in such a way that the distance between the buoy and the beginning (end) of the drift difference vector represents the drift vector before (after) the front passage. Passage times (in UTC) are given by the black numbers. The thick dashed line is the approximate position of the front at 16 UTC. For reference the flight pattern of research aircraft Falcon (between 10 and 12 UTC) is also indicated.

we use this pre-information to determine the time when the front passed over six buoys in the afternoon of this day. The passage is defined as the time when the SLP at the buoys began to rise steeply. In Fig. 12 the frontal passage times for the six buoys are indicated and the approximate front location at 16 UTC is sketched. Buoy passage times underline once more the very slow propagation of the front. Furthermore, the differences of SST and buoy drift calculated for a 6 h time interval (3 h after minus 3 h before the front passage) are given in Fig. 12. The SST changes were not uniform. The ΔSST values varied between −0.8 and +0.1 K; at four of the six buoys ΔSST was negative. The SST changes cannot arise from the sensible and latent heat loss of the ocean for two reasons: (a) the heat loss acts only towards negative ΔSST and (b) even a heat loss of 400 W m^{-2} (the maximum values of $H + E$ observed by aircraft) can change the temperature of a 10 m deep ocean layer by only −0.1 K d^{-1}. Thus, there must be other processes which caused the observed buoy SST changes.

The passage of the front was associated with a systematic change of the drift vector (Fig. 12). This is further detailed in Fig. 13. Fig. 13a shows the trajectories of all 21 XAN-1 buoys over a 6-d period from 10 to 15 March 2005 at hourly time resolution. A coherent drift pattern is not discernible in the experimental area. Instead, the drift appears to be chaotic with mesoscale eddy circulations both in cyclonic and anticyclonic directions. The drift of the above-mentioned six buoys in the vicinity of the wind front is presented with higher spatial resolution in Fig. 13b. The trajectories of these buoys exhibit a sharp kink when the wind front passed. The drift vector difference was similar at all six buoys (Fig. 12) and indicates a similar impact of the wind front on the drift. However, the drift vector field after the frontal passage remained inhomogeneous as it was before the passage. Inhomogeneity must also be concluded to hold for the divergence of the drift. It is mentioned here that the form drag effect on the buoy drift caused by the overwater part of the buoy has been eliminated according to Pazan and Niiler (2001) using the 10 m wind from the ECMWF analyses.

The wind front passed over an ocean which was differently stratified in temperature and salinity in different parts of the experimental area. This is demonstrated in Fig. 14 by CTD measurements taken by R/V Celtic Explorer which—as mentioned above—encircled the experimental area with CTD measurements at positions given in Fig. 13. Only those CTD profiles on the SW side between 68 and 69°N and on the NE side between 71 and 72°N of the experimental area are selected in Fig. 14 because they were located at positions where the wind front passed over two of the six buoys aligned along the wind front in Fig. 12. The selected CTD profiles were located on the W side and E side of the warm water core of the Norwegian Current (NC). They were not taken simultaneously with the wind front. The CTD profiles show different vertical structures which we believe are characteristic of both locations and, thus, are essentially also valid during the wind front passage. On the W side of the NC the oceanic mixed layer reached down to 300–500 m depth. Several profiles show that an internal sub-layer was present in the uppermost 20–100 m which was up to 0.3 K warmer and

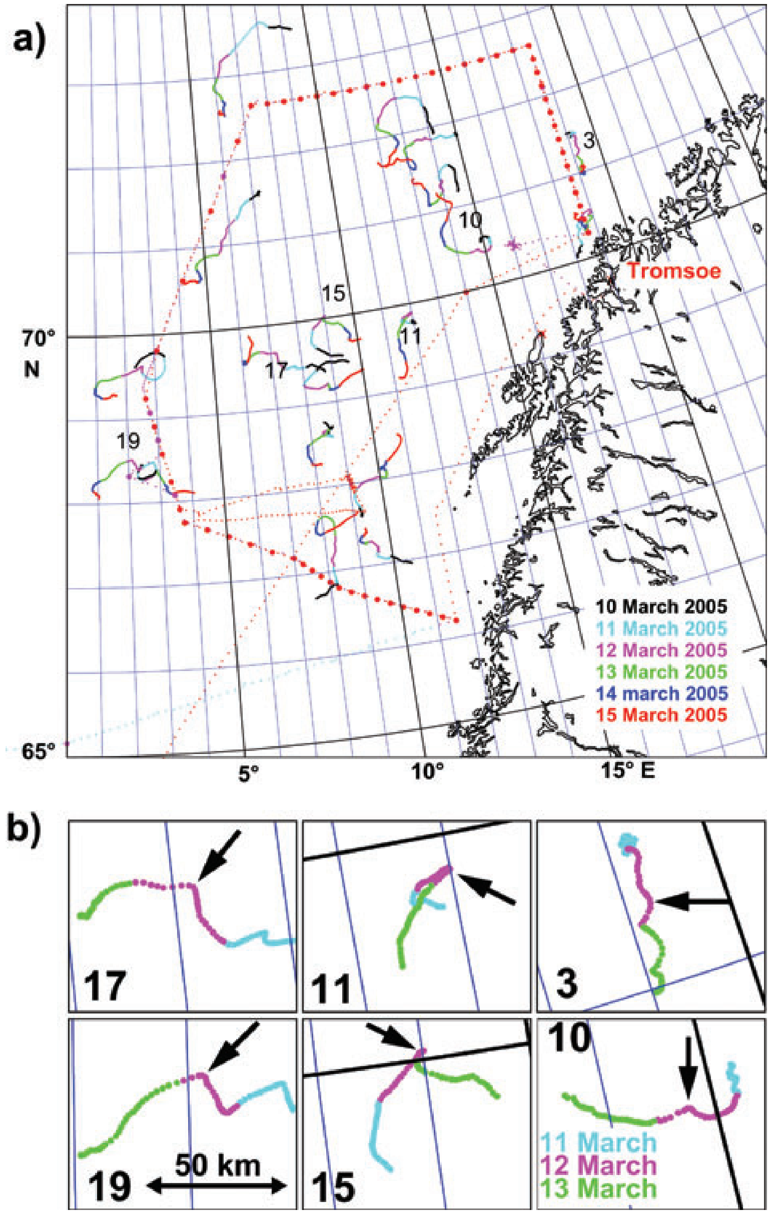

Fig. 13. (a) Drift trajectories of all 21 XAN-1 buoys from 10 to 15 March 2005 at one-hourly time resolution. The six buoys (No. 3, 10, 11, 15, 17 and 19) along the wind front in Fig. 12 are marked. Dotted line represents the track of R/V Celtic Explorer. Full red circles mark CTD profile locations. (b) Drift trajectories of the six buoys along the wind front in higher spatial resolution. Arrows mark time of wind front passage.

limited by a weak thermocline in which the temperature decreased with depth. On the *E* side of the NC, over the shelf area, the mixed layer reached down to the bottom. Here, several profiles show also an internal sublayer in the uppermost 15–100 m which, however, was up to 1 K colder and limited by a sharp thermocline in which the temperature increased with depth. This stratification reflects the influence of the coastal current along the Norwegian coast which is cooler and less haline than the Atlantic water in the core of the NC. Thus, vertical mixing in the ocean would cause SST changes of different sign due to the different vertical stratification of the internal sub-layers in the uppermost 15–100 m on both sides of the NC.

The interpretation of the observed SST change at the buoys in Fig. 12 is furthermore complicated by the existence of SST fronts. This is illustrated in Fig. 15 which shows the SST as measured by the downward looking infra-red radiometer (aperture angle of 2°) aboard the Falcon aircraft during the four wind-front trans-sections H3, H5, H7 and H9. The radiometer recorded several SST steps with amplitudes of some tenths of a degree Kelvin in the experimental area. The infrared SST measurements have to be taken with some restriction because they can be disturbed by precipitation, as it was the case during H7 in a heavy snow shower and when the aircraft had to climb to 70 m height for safety reasons instead of the normal 30 m flight level. However,

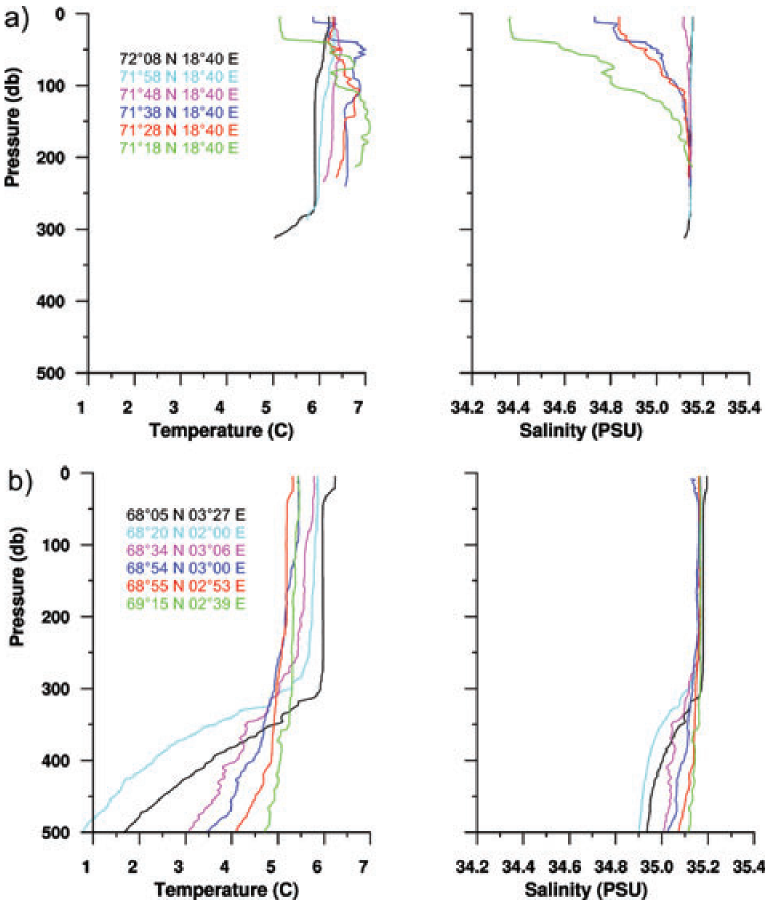

Fig. 14. Vertical profiles of ocean temperature and salinity (a) near buoy No.3 between 71 and 72°N taken on 05 March 2005 between 05 and 11 UTC and (b) near buoy No.19 between 68 and 69°N taken on 01 March 2005 between 02 and 19 UTC. Depth in decibar approximately corresponds to depth in metres.

comparing the SST measurements of the present wind front case with those during other days of the LOFZY field experiment without precipitation we find similar front-like SST steps (not shown). Thus, the measured SST changes at the buoys may also be affected by advection or the drift of the buoy relative to the water mass, although this appears to be very unlikely since the relative drift of the buoy with respect to the water is small. The general existence of SST steps in the area is presumably the effect of the above-mentioned inhomogeneous drift field caused by mesoscale eddies. Nevertheless, the position of the wind front in Fig. 15 is collocated with a SST step. The sign of this step is different in the NE part (H3, H5) and SW part (H7, H9) of the front, but it is in accordance with the opposite temperature stratification in the uppermost 15–100 m of the ocean (Fig. 14) which, in case of vertical mixing, suggests a warming behind the front in the NE part and a cooling in the SW part.

We believe that the observed SST changes at the buoys are primarily caused by the vertical mixing induced by the strong wind front. The strength and the sign are modulated by two further facts: (a) different vertical temperature stratification in the uppermost 15–100 m on both sides of the NC and (b) pre-existing oceanic eddies. Saetra et al. (2008) have shown by model simulation and observation that vertical mixing induced by strong storm events, such as polar lows, is able to cause such SST changes within a few hours. Vertical mixing by Ekman upwelling is also a candidate for SST changes, but appears to be unlikely in our case because it has a much longer time scale on the order of inertial period(s).

6. Summary and conclusions

The characteristics and impact of a storm event which occurred on 12 and 13 March 2005 over the Norwegian Sea is analysed by aircraft, ship, drift buoy and satellite data taken during the LOFZY 2005 field experiment. The storm field with winds up to 27 m s^{-1} was situated on the west-side of a low pressure trough which was aligned along the Norwegian coast and was marked by a sharp wind front. The entire system of trough, wind front and storm field was almost 200 km wide, about 1000 km long, had a long lifetime of almost 2 d, propagated slowly with $c = 1$–3 m s^{-1} southeastwards and, thus, had a long residence time in the area. The total lifetime of the system was nearly 4 d. While the temperature contrast across the system was small (0–4 K) with no front-like structure, the wind contrast was remarkable and occurred as a step-like front with a wind difference of 5–15 m s^{-1} over a distance of 3 km. The wind front

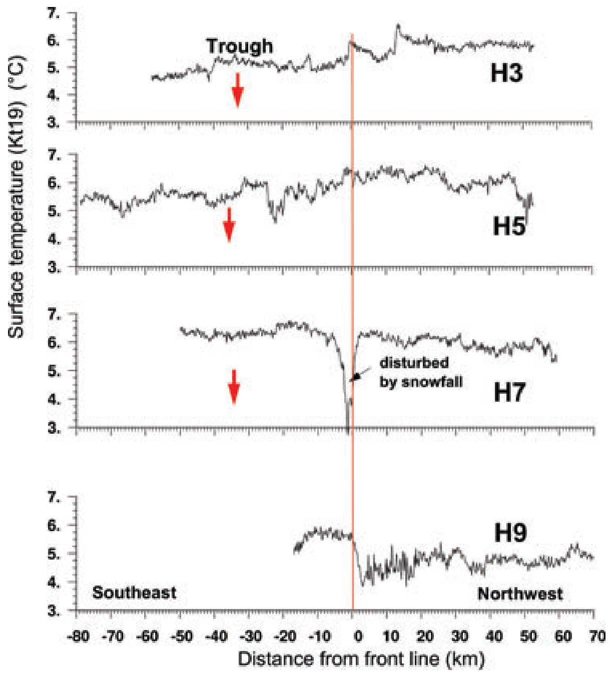

Fig. 15. Sea surface temperature measured by an infrared radiometer aboard research aircraft Falcon along the horizontal flight legs H3, H5, H7 and H9.

was not collocated with the trough, but about 30 km to the NW of it. The front line showed meander-like bulges with about 50 km wavelength probably caused by cross-frontal shear instability. The vertical extent of the storm field was only 1.5–2 km.

The ocean lost heat (sensible plus latent) between 50 W m^{-2} in the trough centre and more than 400 W m^{-2} in the storm field. The heat fluxes in the storm field were about 2.5 times larger than the average wintertime heat flux in this area according to ERA-40 reanalyses (Jahnke-Bornemann, 2009). Net radiation was comparably small. Nevertheless, the turbulent heat losses were too small to account for the observed SST changes between −0.8 and +0.1 K within 6 h during the front passage. The SST changes appear primarily to be the result of vertical mixing induced by the wind front. However, the mixing acted on a temperature stratification in the uppermost 15–100 m of the ocean which was different on both sides of the Norwegian Current: warm water above cooler water on the W side and vice versa on the E side which is influenced by coastal water masses. The impact of the front-induced mixing was additionally modified by the inhomogeneous drift field caused by oceanic eddies. The front caused similar changes of the near-surface drift field, but the eddies continued to exist after the front passage.

The passage of the entire system, trough, front and storm field, was a weak positive freshwater event for the ocean. Based on the aircraft (HOAPS satellite) measurements we estimate an evaporation rate of 0.22 (0.20) mm h^{-1}, a precipitation rate of 0.35 (0.38) mm h^{-1} and thus, a residual freshwater supply of 0.13 (0.18) mm h^{-1}, although the precipitation rate estimate has a large degree of uncertainty due to the known observation problems.

The storm case presented here was an extreme event and we succeeded in sampling data by aircraft at levels as low as 30 m even under wind gusts of 30 m s^{-1}. Although it was an extreme situation, it is obviously not a seldom pressure distribution. Based on the re-analysis data set ERA40, Jahnke-Bornemann (2009) elaborated a cyclone statistics for the area given more or less by the initial buoy rectangle of 400 km times 650 km to the west of the Lofotes Islands and found that a cyclone is present in this area in about 15% of the time. From a visual investigation of the six-hourly SLP analyses produced by Met Office (the UK Meteorological Office) for the year 2005, we find a similar storm field situation as presented here in about 6% of the time. Furthermore, from a visual inspection of the wind field in the twice daily HOAPS climatology between 1988 and 2005, 40 similar wind front events in the Norwegian Sea with a lifetime between 1 and 4 d and wind speeds exceeding 20 m s^{-1} were counted. With these occurrence frequencies in mind, the case described here is among the rare cases, but belongs to a class of strong events which altogether appear to have a climatologic relevance concerning the impact on the upper ocean.

9. Acknowledgments

This research was funded by the German Science Foundation (DFG) under grant SFB 512 “Cyclones and the North Atlantic climate system”. The SeaWinds on QuikSCAT ocean wind data were obtained from the Physical Oceanography Distributed Active Archive Center (PO.DAAC) at the NASA Jet Propulsion Laboratory, Pasadena, CA. ENVISAT-ASAR data were kindly provided by the European Space Agency (ESA).

References

Affeld, B. 2003. Zyklonen in der Arktis und ihre Bedeutung für den Eistransport durch die Framstraße. PhD Thesis, Univ. of Hamburg, Germany 130 pp.

Andersson, A. 2009. The HOAPS climatology: evaluation and applications. PhD Thesis, Univ. of Hamburg, Germany 177 pp.

Brümmer, B., Thiemann, S. and Kirchgäßner, A. 2000. A cyclone statistics for the Arctic based on European Centre re-analysis data. *Meteorol. Atmos. Phys.*, **75**, 233–250.

Cavalieri, D. and Häkkinen, S. 2001. Arctic climate and atmospheric planetary waves. *Geophys. Res. Lett.*, **28**, 791–794.

Drennan, W.M., Zhang, J.A., French, J.R., McCormick, C. and Black, P.G. 2007. Turbulent fluxes in the hurricane boundary layer. Part II: Latent heat flux. *J. Atmos. Sci.* **64**, 1103–1115.

Fairall, C.W., Bradley, E.F., Hare, J.E., Grachev, A.A. and Edson, J.B. 2003. Bulk parameterization of air-sea fluxes: Updates and verification of the COARE algorithm. *J. Climate* **16**(4), 571–591.

French, J.R., Drennan, W.M., Zhang, J.A. and Black, P.G. 2007: Turbulent fluxes in the hurricane boundary layer. Part I: Momentum flux. *J. Atmos. Sci.* **64**, 1089–1102.

Horstmann, J. and Koch, W. 2005. Measurements of ocean surface winds using synthetic aperture radars. *IEEE J. Ocean. Eng.* **30**, 508–515.

Jahnke-Bornemann, A. 2009. Zyklonen im Europäischen Nordmeer. *Variabilität und Zusammenhänge mit der großräumigen atmosphärischen Zirkulation*. PhD Thesis, Univ. of Hamburg, Germany, 115 pp.

Jahnke-Bornemann, A. and Brümmer, B. 2009. The Iceland – Lofotes pressure difference: different states of the North Atlantic low pressure zone. *Tellus* **61A**, 466–475.

Klepp, C., Bumke, K. and Bakan, S. 2010. Ground validation of oceanic snowfall in satellite climatologies during LOFZY. *Tellus* **62A**, this issue.

Lammert, A., Brümmer, B., Ebbers, I. and Müller, G. 2008. Validation of ECMWF and DWD model analyses with buoy measurements over the Norwegian Sea. *Meteorol. Atmos Phys.* **102**, 87–96.

Moore, G.W.K., Pickart, R.S. and Renfrew, I.A. 2008. Buoy observations from the windiest location in the world ocean, Cape Farewell, Greenland. Geophys. *Res. Lett.* **35**, L18802, doi:10.1029/2008GL034845.

Pazan, S.E and Niiler, P.P. 2001. Recovery of near-surface velocity from undrogued drifters. *J. Atmos. Oceanic Tech.* **18**(3), 476–489.

Petersen, G.N. and Renfrew, I.A. 2009. Aircraft-based observation of air-sea fluxes over Denmark Strait and the Irminger Sea during high wind speed conditions. *Q.J.R. Meteor. Soc.* **135**, 2030–2045.

Persson, P.O.G., Hare, J.E. Fairall, C.W. and Otto, W.D. 2005. Air-sea interaction processes in warm and cold sectors of extratropical cyclonic storms observed during FASTEX. *Q.J.R. Meteor. Soc.* **131**, 877–912.

Pickart, R.S., Spall, M.A., Hvid Ribergaard, M., Moore, G.W.K. and Milliff, R.F. 2003. Deep convection in the Irminger Sea forced by the Greenland tip jet. *Nature* **424**, 152–156.

Poulain, P.M., Warn-Varnas, A. and Niiler, P.P. 1996. Near-surface circulation of the Nordic Seas as measured by Lagrangian drifters. *J. Geophys. Res.* **101**(C8), 18237–18258.

Renfrew, I.A., Petersen, G.N., Sproson, D.A.J., Moore, G.W.K., Adiwidjaja, H. and co-authors. 2009. A comparison of aircraft-based surface-layer observations over Denmark Strait and the Irminger Sea with meteorological analyses and QuikSCAT winds. *Q. J. R. Meteor. Soc.* **135**, 2046–2066.

Ren, X., Perrie, W., Long, Z. and Gyakum, J. 2004. Atmosphere-ocean coupled dynamics of cyclones in midlatitudes. *Mon. Wea. Rev.* **132**, 2432–2451.

Rogers, J.C. 1997. North Atlantic storm track variability and its association to the North Atlantic oscillation and climate variability of Northern Europe. *J. Climate* **10**, 1635–1647.

Saetra, O., Linders, T., Debernard, J.B. 2008. Can polar lows lead to a warming of the ocean surface? *Tellus* **60A**, 141–153.

Schade L.R. and Emanuel, K.A. 1999. The ocean's effect on the intensity of tropical cyclones: Results from a simple coupled atmosphere-ocean model. *J. Atmos. Sci.* **56**, 642–651.

Skeie, P. 2000. Meridional flow variability over the Nordic Seas in the Arctic oscillation framework. *Geophys. Res. Lett.* **27**, 2569–2572.

Sorteberg, A., wamto, N.G. K. and Byrkjedal, D. 2005. Wintertime Nordic Seas cyclone variability and its impact on oceanic volume transports into the Nordic Seas. In: *The Nordic Seas* (eds Drange and co-editors), AGU Monograph, 137–157.

Tsukernik, M., Kindig, D. and Serreze, M. 2007. Characteristics of winter cyclone activity in the Northern North Atlantic: Insights from observations and regional modeling. *J. Geophys. Res.* **112**, D03101, doi:10.1029/2006jd007184.

Young, G.S., Sikora, T.D. and Winstead, N.S. 2005. Use of synthetic aperture radar in finescale surface analysis of synoptic-scale fronts at sea. *Wea. Forecast.* **20**, 311–327.

Zhang, X., Walsh, J., Zhang, J., Bhatt, U. and Ikeda, M. 2004. Climatology and interannual variability of Arctic Cyclone activity: 1948–2002. *J. Climate* **17**, 2300–2317.

Zedler, S.E., Dickey, T.D., Doney, S.C., Price, J.F., Yu, X. and coauthors. 2002: Analyses and simulations of the upper ocean's response to hurricane Felix at the Bermuda Testbed Mooring site: 13–23 August 1995. *J. Geophys. Res.* **107**(C12), 3232, doi:10.1029/2001JC000969.